PCCP

Physical Chemistry Chemical Physics

www.rsc.org/pccp

Volume 11 | Number 1 | 7 January 2009 | Pages 1–196

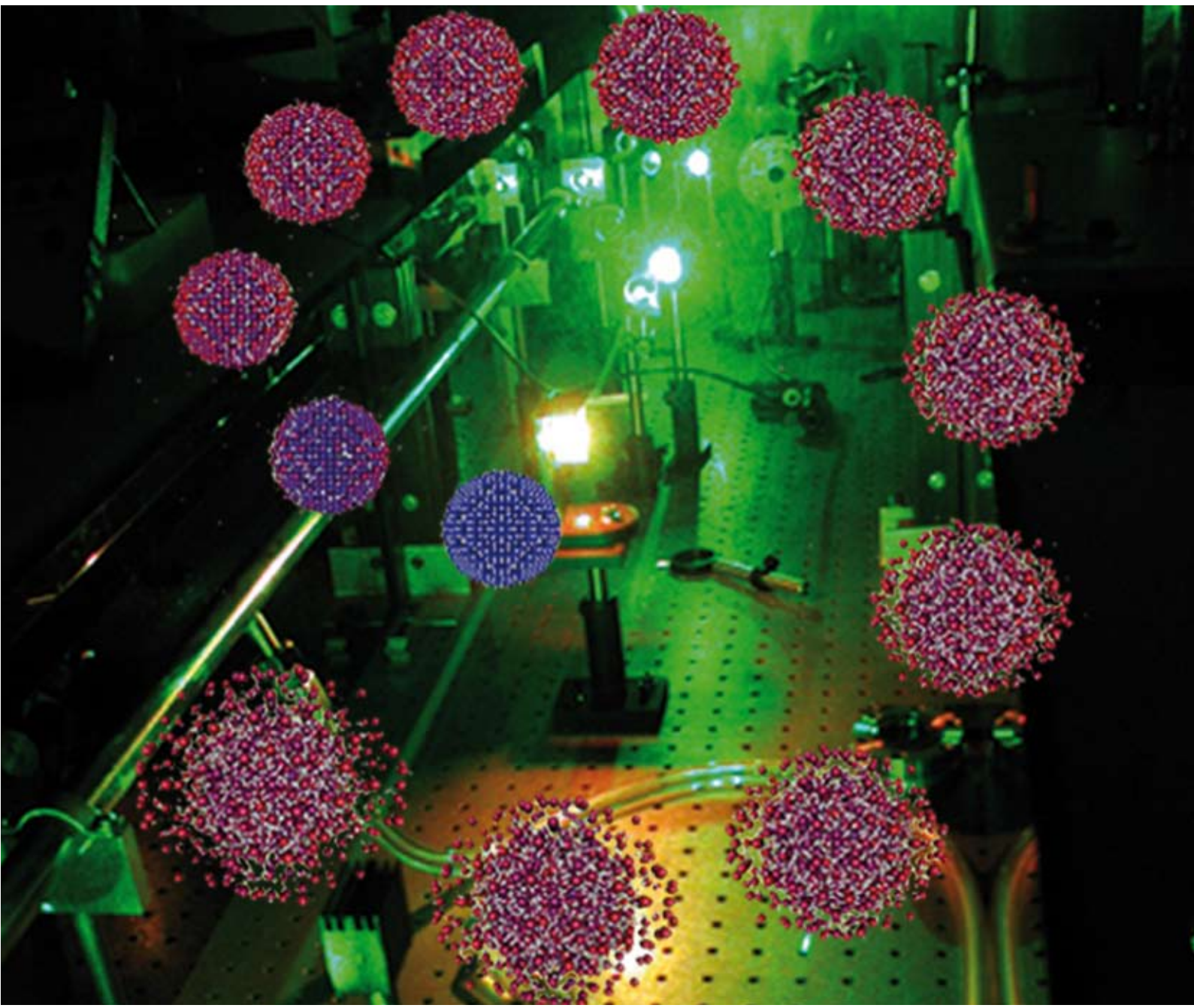

ISSN 1463-9076

COVER ARTICLE
Jortner *et al.*
Extreme dynamics and energetics of Coulomb explosion of Xe clusters

PERSPECTIVE
Haran *et al.*
Collapse transition in proteins

1463-9076(2009)11:1;1-8

Extreme dynamics and energetics of Coulomb explosion of Xe clusters

Andreas Heidenreich,[a] Isidore Last[b] and Joshua Jortner[b]

Received 28th October 2008, Accepted 17th November 2008
First published as an Advance Article on the web 24th November 2008
DOI: 10.1039/b819126n

Unique features of Coulomb explosion (CE) of many-electron elemental Xe_n (n = 13–2171) clusters driven by ultraintense and ultrashort near-infrared laser pulses (peak intensities 10^{15}–10^{20} W cm^{-2} and pulse lengths of 10–100 fs) manifest ion dynamics and energetics in the extreme, with ultrafast (5–15 Å fs^{-1}) velocities and ultrahigh (keV–1 MeV) energies. Relations were established between the CE attributes, obtained from molecular dynamics simulations and from electrostatic models, and the extreme cluster inner ionization levels (5–36 per ion), in conjunction with the laser parameters required for the attainment of complete outer ionization, which was approximated by cluster vertical ionization (CVI) initial conditions. Interrelationship between electron dynamics and nuclear dynamics stems from the effects of the laser pulse length on the energetics and from the characterization of the border radius for complete outer ionization. Our computational-theoretical analysis semi-quantitatively describes CE dynamics and energetics in the CVI limit and also the energetics in the presence of a persistent nanoplasma, which is in accord with experiment.

1. Introduction

The exploration of the Coulomb instability of large, finite, multicharged systems constitutes a long-standing challenge in the fields of chemistry, physics and biophysics.[1–3] The study of Coulomb instability of clusters was initiated by Castleman *et al.* for Coulomb explosion (CE) of molecular clusters,[4] and by Recknagel *et al.*[5] and Bréchignac *et al.*[6] for fission of metal clusters. Related work focused on a momentum-resolved survey of the Rayleigh fission barrier in rare gas clusters[7] and on CE of proteins.[3] Extreme Coulomb instability resulting in CE[2] is manifested by multiple ionization of elemental and molecular clusters, *e.g.*, Ar_n, Xe_n, $(H_2)_n$, $(D_2)_n$, $(H_2O)_n$, $(D_2O)_n$, $(CH_4)_n$, $(CD_4)_n$, $(DI)_n$, and $(CD_3I)_n$ in ultraintense laser fields (peak intensity I_M = 10^{15}–10^{20} W cm^{-2}).[8–11] Subsequent cluster CE then results in the production of highly energetic (keV–MeV) multicharged ions (*e.g.*, H^+, D^+, C^{q+} (q = 4–6), O^{q+} (q = 6–8), I^{q+} (q = 25) and Xe^{q+} (q = 5–36)).[8–27] CE of deuterium clusters[12–15] and of deuterium containing heteroclusters[16–24] drives dd nuclear fusion within and outside the plasma filament formed in an assembly of exploding $(D_2)_n$, $(CD_4)_n$, $(D_2O)_n$ or $(DI)_n$ clusters, with the production of neutrons.[12–24] CE of assemblies of completely ionized large $(CH_4)_n$, $(NH_3)_n$ and $(H_2O)_n$ clusters (nanodroplets) will drive nucleosynthesis of protons with $^{12}C^{6+}$, $^{14}N^{7+}$ and $^{16}O^{8+}$ nuclei, with γ ray production,[28,29] which is of interest for nuclear astrophysics.[28] Notable potential applications of the table-top devices based on cluster CE pertain to ion imaging,[30] accelerator technology of high-energy ions and nuclei,[31] extreme ultraviolet lithography,[32] dd nuclear fusion,[12–24] nucleosynthesis,[28,29] time-resolved neutron diffraction[14] and ultrafast γ ray emission.[29]

Theoretical models and computer simulations[8–11,15,17,18,22–29,33–37] considered CE dynamics of multicharged clusters driven by a sequential-parallel series of processes involving cluster multiple inner ionization, the formation and response of a nanoplasma within the cluster or in its vicinity and cluster outer ionization.[8–10] Electrostatic models addressed the energetics and dynamics of uniform CE of homonuclear clusters (with equal charge on each atom) under conditions of cluster vertical ionization (CVI), where the transient nanoplasma is completely depleted by outer ionization[10,33,34] with the production of an ionic cluster at the initial nuclear configuration of the neutral cluster. Additional applications of electrostatic models involved non-uniform CE of heteroclusters[23–24,34] and a description of CE when the nanoplasma is persistent.[35] A useful concept for the characterization of complete outer ionization and for the specification of the conditions for the prevalence of a transient or a persistent nanoplasma involves the (laser intensity and pulse length dependent) border radius $R_0^{(I)}$.[33–34,36] Computational information on cluster multiple ionization, electron dynamics and CE emerged[8–11,15,17,18,22–29,37] from particle molecular dynamics (MD) simulations, which are practical for clusters containing up to n = 10^3–10^4 atomic/molecular constituents,[25,27,37] and from a scaled MD procedure, which is applicable for nanodroplets containing up to n = 10^6–10^7 constituents.[38]

In this paper we present a computational and theoretical study of CE of elemental Xe_n clusters (n = 13–2171) driven by Gaussian laser fields in the intensity range I_M = 10^{15}–10^{20} W cm^{-2}. Experimental information is available on the energetics of CE of Xe_n clusters in the broad size domain of n = 200–8 × 10^4 and in the intensity range of 3 × 10^{15}–2 × 10^{17} W cm^{-2}.[13,39,40] The dynamics and energetics of the ions and of the (high-energy) electrons were studied herein by MD simulations, using the computational methods including a relativistic treatment of the electrons previously described.[25,27,37] This MD simulation code[37]

[a] *Institut für Chemie, Humboldt-Universität zu Berlin, Brook-Taylor-Str. 2, D-12489 Berlin, Germany*
[b] *School of Chemistry, Tel Aviv University, Ramat Aviv, 69978 Tel Aviv, Israel*

is applicable for extreme inner ionization, multielectron dynamics, nanoplasma formation and response, cluster outer ionization and nuclear CE dynamics in elemental and molecular clusters driven by ultraintense laser fields.[25–27,33–34,37] The validity conditions for the applicability of classical MD simulations to high-energy electron dynamics rest on the localization of the electron wavepacket and on the neglect of quantum permutation symmetry constraints for identical (plasma) particles.[37] The Xe_n clusters were coupled to a near-infrared ($\nu = 0.35$ fs^{-1}, $h\nu = 1.44$ eV) Gaussian laser field (pulse length of τ = 10–100 fs). The laser pulse was characterized by the initial time $t = t_s$ ($t_s < 0$) for the switching on of the field,[25,37] the time $t = 0$ for the maximum of the field envelope, $t = -t_s$ for the termination of the pulse and $t = t_L$ ($t_L = 4\tau$) for long times. Some new facets of nuclear dynamics of CE of highly charged elemental clusters of many-electron Xe atoms are revealed:

(1) The dependence of the dynamics and energetics of CE of many electron elemental clusters on the cluster size and on the laser parameters. Extreme multiple ionization produces $\{Xe^{q+}\}_n$ clusters, with an average charge q_{av} per atom of q_{av} = 5–36,[25,27,40,41] allowing for the interrogation of CE attributes over a broad domain of ionic charges.

(2) CE under complete outer ionization. In the cluster size domain ($n \leq 2171$) studied herein and at sufficiently high laser intensities ($I_M = 10^{18}$–10^{20} W cm^{-2}) the nanoplasma will be transient, undergoing complete outer ionization with the formation of a purely ionic cluster.[25–27,36] A limiting case of this physical situation involves CE under CVI conditions, which constitutes a purely ionic system in the geometry of the neutral cluster.[25,26,33,34] Electrostatic models for CE energetics and dynamics under CVI conditions accounted for the gross features of the simulation results for $I_M \geq 10^{18}$ W cm^{-2}.

(3) CE under incomplete outer ionization. At lower intensities ($I_M = 10^{15}$–10^{16} W cm^{-2}) and/or large cluster sizes the nanoplasma is persistent, retarding CE due to screening effects. The dependence of the CE energetics for these conditions was accounted for by a persistent "cold" nanoplasma model,[35] which was extended for many-electron clusters.

(4) The characterization of electron outer ionization and CE nuclear energetics in terms of the laser intensity and pulse length dependence of the border radius $R_0^{(I)}$. In our previous work[10,24,33,34,36] for sufficiently short pulses ($\tau \leq 25$ fs), $R_0^{(I)}$ was evaluated from modeling[33,34,36] and from simulations of outer ionization electron dynamics at the laser peak.[33,36] In the present work, the dependence of $R_0^{(I)}$ on the laser parameters (over the intensity range $I_M = 10^{15}$–10^{17} W cm^{-2} and over the pulse length domain of τ = 25–100 fs) was determined from two independent sources. First, we determined $R_0^{(I)}$ from simulations of outer ionization dynamics and yields, which modifies and extends the formalism previously given by us.[24,33,34,36] Second, $R_0^{(I)}$ was determined from simulation results for the energetics of CE, which manifests the onset of the deviations from the R_0^2 scaling laws.[8,10,24,33,34] The results for outer ionization yields and CE energetics were confronted with the predictions of the electrostatic model for complete cluster barrier suppression ionization (CBSI).[25,36] This analysis for $R_0^{(I)}$ provides relations between the energetics of CE and electron outer ionization of many-electron elemental clusters.

II. Gross features of CE of Xe_n clusters

II.A Time-resolved structures

The characteristics of the parallel-sequential processes of electron and nuclear dynamics are demonstrated for Xe_{2171} clusters coupled to an infrared Gaussian laser pulse at intensities $I_M = 10^{15}$ W cm^{-2} (Fig. 1) and $I_M = 10^{18}$ W cm^{-2} (Fig. 2). Snapshots of the time evolution at the lower intensity of $I_M = 10^{15}$ W cm^{-2} (Fig. 1) reveal time-dependent inner ionization with the formation of Xe^{q+} ions in the range of q = 1–9, with the ion charges increasing during 40 fs (Fig. 1). Inner ionization results in the formation of a nanoplasma, part of which is stripped from the cluster by outer ionization, while a large fraction (75%) of these electrons remain within the cluster, forming a persistent nanoplasma (Fig. 1). The cluster consists of two charged parts: a neutral central sphere containing the persistent nanoplasma and a fully outer ionized peripheral sphere containing ions. The CE sets in at $\sim$50 fs after the onset of the laser pulse (Fig. 1), involving the

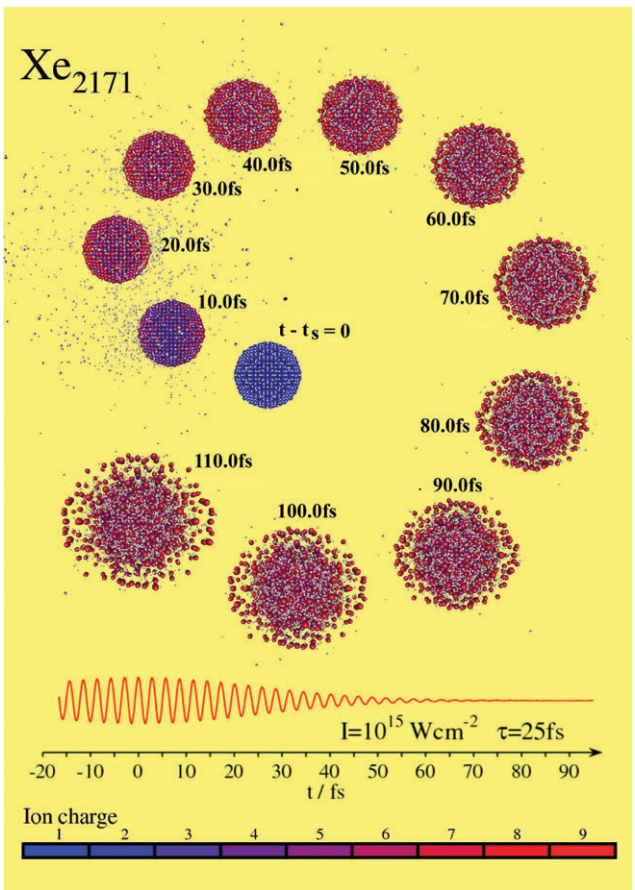

Fig. 1 Snapshots of the time-resolved inner ionization, nanoplasma response, charge distribution, outer ionization and Coulomb explosion of a Xe_{2171} cluster driven by a Gaussian laser pulse with $I_M = 10^{15}$ W cm^{-2} and τ = 25 fs, with the electric field of the laser being shown in the lower part of the panel. The times that mark the snapshots correspond to the values of $t - t_s$ (where t_s is the initial time for switching on of the field). The Xe ions are color coded according to their charge, and the electrons are represented by light gray spheres.

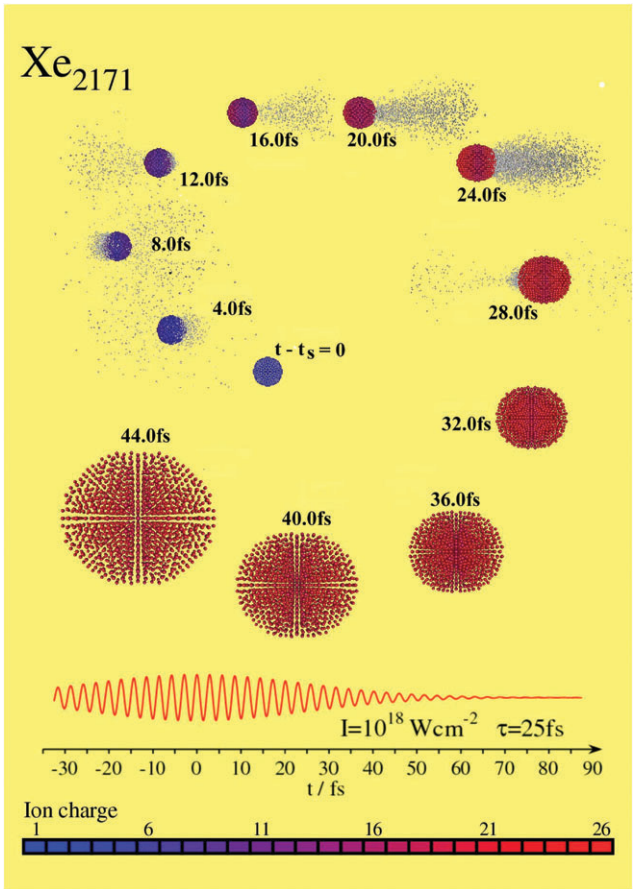

Fig. 2 Snapshots of the time-resolved electron and nuclear dynamics of a Xe_{2171} cluster driven by a Gaussian laser pulse with I_M = 10^{18} W cm^{-2} and τ = 25 fs. Presentation as in Fig. 1.

peripheral ionic sphere and being considerably faster for the peripheral ions. Over the longer time scale of 50 fs to 90 fs, the radius of the sphere of the persistent nanoplasma stays nearly constant, while the peripheral nuclear framework of the ions does expand, in accord with the 'lychee model'.[35] Snapshots of the time evolution at the higher intensity of I_M = 10^{18} W cm^{-2} (Fig. 2) reveal time-dependent inner ionization with q = 1–26, with the ion charges markedly increasing during 30 fs (Fig. 2). In this intensity domain, the nanoplasma is transient, with all its electrons being stripped from the cluster by outer ionization, which is complete at 32 fs (Fig. 2). CE becomes marked at about 24 fs (Fig. 2), occurring in parallel to outer ionization. Cluster CE is considerably faster for the transient nanoplasma (Fig. 2) than in the presence of a persistent nanoplasma (Fig. 1). The cluster structures seem to exhibit also some layer or channel structures, in particular at 36–44 fs in Fig. 2, giving an impression that the CE induces such structural changes of the initial fcc structure. However, a closer inspection shows that the "channels" can be also seen in the initial undistorted fcc geometry, showing that the "channels" are spurious and their appearance is caused by the perspective of the 3D graphics. Both at I_M = 10^{15} W cm^{-2} and at I_M = 10^{18} W cm^{-2} (Fig. 2), the CE manifests anisotropy in the angular distribution of the Xe^{q+} ions, which is due to the driving of the ions by the nanoplasma electrons,[33] with the cluster expansion at longer times being ellipsoidal in the direction of the laser electric field. This phenomenon will be analyzed elsewhere.[42]

II.B Time dependent distribution of Xe^{q+} ions

Inner/outer cluster ionization results in the production of $\{Xe^{q+}\}_n$ ions with a cluster size, laser intensity and pulse length dependent distribution {q} of the ionic charges. The spatial charge-resolved density function $n(q,r)$ of the Xe^{q+} ions of charge q within a spherical shell Δr at a distance r from the cluster center was presented for intervals Δr, with $\Delta r/R_{CUT}$ = 0.05, where R_{CUT} is the cut-off radius of the distribution. $n(q,r)$ obeys the normalization condition $\sum_r n(q,r)\Delta r$ = $n(q)$, where $n(q)$ denotes the density function of ions of charge q. The spatial total distribution, $n(r)$, of all the ions (per Xe atom) at distance r is given by $n(r)$ = $\sum_q n(q,r)$, with the normalization condition $\sum_r n(r)\Delta r$ =1. Information on the femtosecond dynamics of CE is inferred from the time dependence of the charge resolved distribution $n(q,r)$ and the total distribution $n(r)$. In Fig. 3 we present the time-resolved data for $n(r)$ for CE of a Xe_{2171} cluster, which manifest the marked effects of the intensity of the driving of laser on the CE dynamics. The initial cluster atom distribution (at t = t_s) is characterized by $R_{CUT}(t_s)$ = 34 Å (Fig. 3), which is close to the initial cluster radius R_0 = 31 Å.

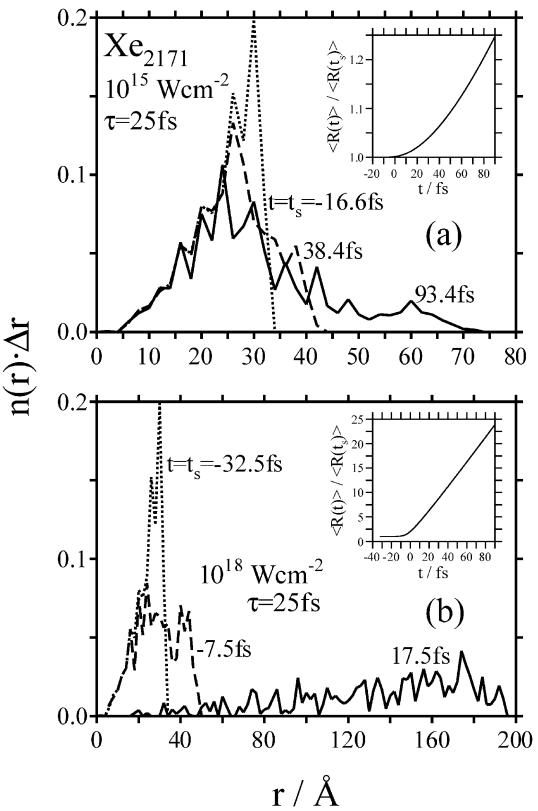

Fig. 3 Time dependence of the radial density function $n(r)$ of Xe ions from Xe_{2171} clusters, driven by Gaussian pulses with τ = 25 fs, for the times given at the curves, with the initial time t = t_s. (a) I_M = 10^{15} W cm^{-2} and (b) I_M = 10^{18} W cm^{-2}. The insets show the time-dependent first moments of the distribution functions, normalized to the first moment $\langle R(t_s)\rangle$ at the initial time t_s.

At $I_M = 10^{15}$ W cm^{-2} ($\tau = 25$ fs) the spatial expansion of $n(r)$ (Fig. 3a) exhibits a bimodal distribution, consisting of the two components: (i) a close proximity peak in the spatial range $r_{MAX} = 25$–30 Å, whose position is nearly time independent; (ii) a long-distance tail with $R_{CUT} = 44$ Å at $t - t_s = 55$ fs and $R_{CUT} = 75$ Å at $t - t_s = 110$ fs ($t = t_L$). Component (i) corresponds to the persistent and almost neutral nanoplasma, while component (ii) represents the CE of the exterior ions. The bimodal distribution manifests non-uniform CE at $I_M = 10^{15}$ W cm^{-2}. For $\tau = 25$ fs, the examination of the long–time charge distribution $n(q,r)$ at $t = t_L$ (Fig. 4(a)) reveals that for this short pulse length the largest values of the charges, *i.e.*, $q = 7$–9, appear at the exterior of the cluster, where ignition barrier suppression ionization (BSI) effects for inner ionization[25,27] are important. These highly charged exterior ions contribute to component (ii) of CE. For longer pulse lengths ($\tau = 100$ fs at $I_M = 10^{15}$ W cm^{-2}) a major change of the charge distribution is manifested (Fig. 4(b)), where the higher charges $q = 10,11$ are dominant in the cluster center, due to the enhancement of inner ionization *via* electron impact ionization (EII) at long τ.[27,43] Under these conditions, component (i) of the persistent nanoplasma (which peaks in the range 50–60 Å) involves the higher charged ions, while component (ii) of CE constitutes the lower charged peripheral ions. Thus the nature of the ions undergoing CE of the exterior shells at $I_M = 10^{15}$ W cm^{-2} depends on the pulse width, being determined by the interplay between ignition and EII mechanisms.

At $I_M = 10^{18}$ W cm^{-2} ($\tau = 25$ fs), inner ionization (to $q_{av} = 23$) is completed at $t - t_s = 35$ fs (Fig. 2), while effective CE sets in at $t - t_s \geq 25$ fs (Fig. 3(b)), taking place in parallel to outer ionization. The nanoplasma is transient (Fig. 2), inducing efficient CE (Fig. 3(b) and 5(b)). At $t - t_s = 50$ fs, $n(r)$ reveals a broad ion distribution, being manifested in the range $r = 20$–200 Å (Fig. 3(b)), with a considerable expansion $R_{CUT}/R_{CUT}(t_s) = 6.5$, manifesting CE under conditions of complete outer ionization. At this high intensity, the

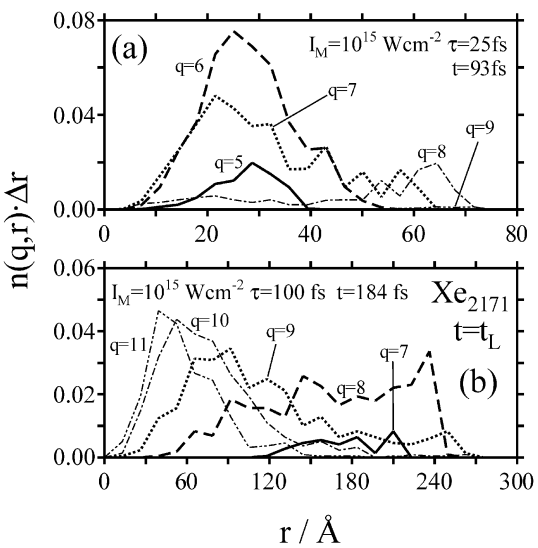

Fig. 4 The radial density functions n(q,r) of Xe^{q+} ions at time t_L (end of trajectory) for Xe_{2171} driven by Gaussian pulses with $I_M = 10^{15}$ W cm^{-2}, for different pulse lengths: (a) $\tau = 25$ fs, (b) $\tau = 100$ fs.

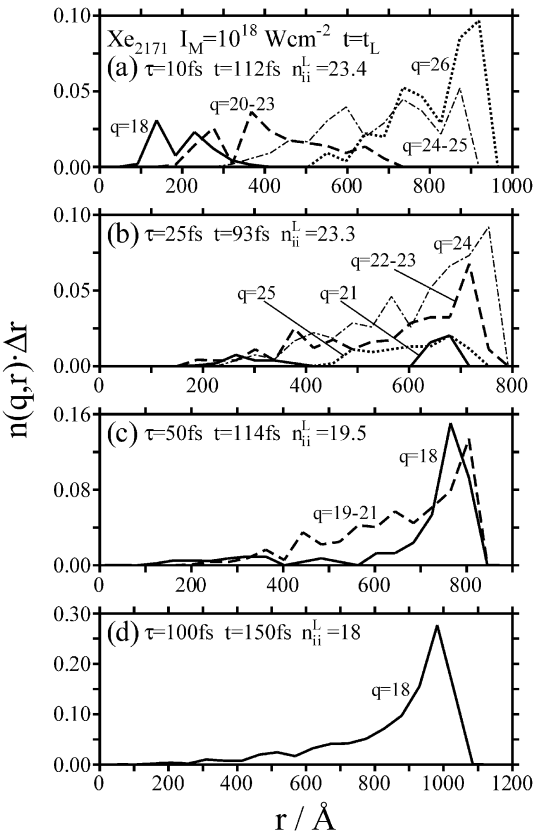

Fig. 5 The radial density functions $n(q,r)$ of Xe^{q+} ions at time t_L for Xe_{2171} driven by a Gaussian laser pulse with $I_M = 10^{18}$ W cm^{-2}, for different pulse lengths: (a) $\tau = 10$ fs, (b) $\tau = 25$ fs, (c) $\tau = 50$ fs, and (d) $\tau = 100$ fs.

charge-resolved spatial distributions with $q = 21$–25 exhibit a marked CE, with $R_{CUT}/R_{CUT}(t_s) = 23$ at $t - t_s = 120$ fs ($t = t_L$), with all the cluster ions exhibiting a concurrent, nearly uniform CE (Fig. 5(b)). The qualitatively different time scales for CE at different intensities are shown in the insets of Fig. 3(a) and (b), which present the time dependence of the first moments $\langle R(t)\rangle$ of $n(r)$ at time t, which are normalized to their initial values $\langle R(t_s)\rangle$. At $I_M = 10^{15}$ W cm^{-2} the non-uniform CE is slow, with $\langle R(t)\rangle/\langle R(t_s)\rangle = 1.25$ at $\tau = 90$ fs, while at $I_M = 10^{18}$ W cm^{-2} the nearly uniform CE is considerably faster with $\langle R(t)\rangle/\langle R(0)\rangle = 24$ at $t = 90$ fs. We shall return to this point in section III.

Of interest is the pulse length dependence (at fixed I_M) of the ionic charges and of the radial charge ordering in an exploding Xe_{2171} cluster driven by a ultrahigh-intensity laser with $I_M = 10^{18}$ W cm^{-2} (Fig. 5). Increasing the laser pulse length from $\tau = 10$ fs to 100 fs results in a marked decrease of the long-time maximal charge $n(q,r)$ from $q = 26$ for $\tau = 10$ fs (Fig. 5a) to $q = 18$ for $\tau = 100$ fs at $t = t_L$ (Fig. 5d). For the shorter pulse lengths a moderately broad distribution of ionic charges is produced, *i.e.*, $q = 18$–26 for $\tau = 10$ fs (Fig. 5(a)) and $q = 21$–25 for $\tau = 25$ fs (Fig. 5(b)). On the other hand, for the longer pulse of $\tau = 100$ fs, a single ionic charge of $q = 18$ is produced (Fig. 5(d)). For shorter pulses of $\tau = 10$ fs and $\tau = 25$ fs, the increase of the maximal and dominating ionic charge above the atomic limit of $q = 18$ to $q = 25$ (for $\tau = 25$ fs) and to $q = 26$ (for $\tau = 10$ fs) is due to the ignition BSI

mechanism[25,27] (section II.C), which is effective when CE is minor during the short pulse. On the other hand, for the longer pulse of $\tau = 100$ fs, the ignition BSI effects are inoperative due to effective CE during the pulse. Indeed, for $\tau = 100$ fs Xe^{18+} ions, with a single valued charge corresponding to the atomic limit,[35] are produced. Changing the pulse length at $I_M = 10^{18}$ W cm^{-2} reflects on an interplay between the attainment of BSI by the laser electric field and by the intracluster ignition effects.

The simulation results of Fig. 5, which portray the τ dependence of the cut-off radii R at $I_M = 10^{18}$ W cm^{-2}, provide information on long-time CE dynamics. The normalized distances $R/R_{CUT}(t_s)$ (where $R_{CUT}(t_s) = 34$ Å) are increasing on the time scale of $\Delta t = t - t_{onset}$ (where, as discussed in section III, $t_{onset} \approx 1$ fs is the time, relative to the pulse peak, for the completion of outer ionization and for the termination of acceleration effects in Xe_{2171} at this intensity). The velocities of CE, *i.e.*, $[R/R_{CUT}(t_s) - 1]/\Delta t$, are estimated to be 0.245 fs^{-1} at $\tau = 10$ fs and 0.205 fs^{-1} at $\tau = 100$ fs. A more accurate estimate based on the difference between the values of $R(t)/R_{CUT}/t_s$ in the time interval of 2 fs towards the end of the simulations results in CE velocities of 0.247 fs^{-1} and 0.147 fs^{-1} at $\tau = 10$ fs and at $\tau = 100$ fs, respectively. The decrease of the CE velocity with increasing τ is due to the decrease of the ionic charges at longer pulse lengths (Fig. 5).

II.C Ionization levels

For Xe clusters there is no saturation limit for the increase of the Xe ionization level by increasing the laser intensity in the experimentally accessible domain of $I_M \leq 10^{21}$ W cm^{-2}. In Fig. 6 we present the cluster size dependence ($n = 55$–2171), laser intensity dependence ($I_M = 10^{15}$–10^{20} W cm^{-2}), and laser pulse length dependence ($\tau = 10$–100 fs) of the average ionization levels q_{av} (per Xe atom) produced by inner ionization. A report on these data was previously presented by us,[37] and here we shall confine ourselves to a brief analysis of the q_{av} data, which provide a central parameter for CE dynamics and energetics. For a fixed cluster size and for all values of τ, q_{av} increases with increasing I_M, manifesting the contribution of the laser field to BSI. The effects of the charged cluster environment and of the initial cluster size on the inner ionization level will be inferred from the comparison of the cluster q_{av} data with the single atom ionization levels[25] (presented by horizontal arrows in Fig. 6). At the highest intensities of $I_M = 10^{19}$–10^{20} W cm^{-2}, q_{av} is cluster size independent and invariant to changes in τ, being equal to the single atom ionization levels at each intensity (Fig. 6). The increase of q_{av} with increasing the cluster size manifests the ignition BSI effect by the cluster ions, giving rise to the enhancement of the inner field, which contributes to the BSI ignition.[25,27] Typical examples where q_{av} exceeds the single atom value are given at $I_M = 10^{18}$ with $\tau = 10$ fs and 25 fs, and at $I_M = 10^{17}$ W cm^{-2} with $\tau = 50$ fs and 100 fs (Fig. 6). The ignition effect at fixed n and I_M decreases with increasing τ. The decrease of q_{av} with increasing the cluster size manifests the screening effect of the ion field by the nanoplasma electrons,[25,27] being prominent at $I_M = 10^{17}$ W cm^{-2} with $\tau = 25$ fs and at $I_M = 10^{18}$ W cm^{-2} with $\tau = 10$ fs (Fig. 6). Finally, the contribution of EII is important for lower intensities, *i.e.*, $I_M = 10^{15}$ W cm^{-2}, in the ultra-

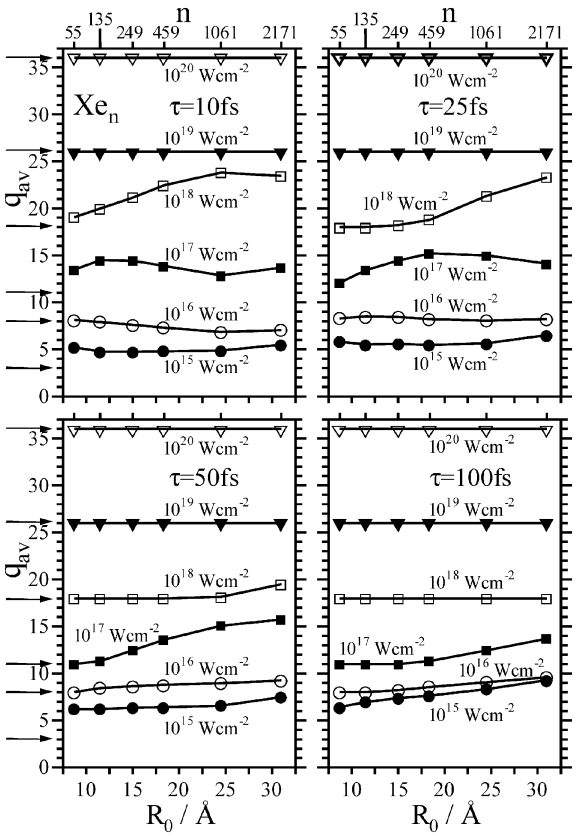

Fig. 6 Cluster size, laser intensity and pulse length dependence of the average charges q_{av} (per ion) for the Xe_n clusters in the intensity range marked on the curves and for the pulse lengths marked on the panels. The horizontal arrows on the left side represent the limit for the single atom ionization level.

intense domain, being significant for long $\tau = 50$–100 fs pulses.[27] This complex interplay between laser field BSI, inner field ignition BSI and nanoplasma screening, and EII effects (Fig. 6) provides input information for the dependence of q_{av} on the cluster size and the laser parameters, which govern CE dynamics (section III) and energetics (section IV) of many-electron heavy-atom Xe_n clusters.

III. Dynamics of Coulomb explosion

CE of homonuclear clusters under CVI conditions often involves uniform ion expansion. This applies for homonuclear clusters with an initially homogeneous, equal ionic charge and spherically symmetric ion distribution, which retains the succession of the hierarchy of the ion distances throughout the expansion, manifesting a unimodal spatial distribution at all times.[10,33,34] Analytic expressions were obtained for the temporal dynamics and energetics of CE under these conditions.[10,24,33] For CE of heteroclusters, *e.g.*, $(A^{q_A+}B^{q_B+})_n$, the dynamics is nonuniform, being governed by a kinematic parameter[17,24,34,44] $\eta = q_A m_B/q_B m_A$. Another origin of nonuniform CE can be exhibited in an elemental cluster with different ionic charges. For CE of Xe_n clusters under CVI conditions of complete outer ionization, which are realized at $I_M > 10^{17}$ W cm^{-2} (section II), a distribution of the ionic charges of Xe^{q+} is often exhibited, *e.g.*, for Xe_{2171} at

$I_M = 10^{18}$ W cm^{-2} (τ = 25 fs) the ionic charges fall in the range q = 21–25 (Fig. 4), with a spread Δq = 5 and $\Delta q/q_{av} \simeq 0.25$. Thus the CE of such clusters is not strictly uniform, with the kinematic parameter for CE of differently charged Xe^{q+} ions exhibiting a value of $\eta = 1 + \Delta q/q_{av} \approx 1.25$. Nevertheless, CE dynamics of $\{Xe^{q+}\}_n$ clusters driven by short pulses (τ = 25 fs) under conditions of complete outer ionization, will be reasonably well approximated by CVI initial conditions, with a uniform CE of $\{Xe^{q_{av}+}\}_n$ clusters.

The CE of Xe_n clusters (Fig. 3 and 7) was characterized by the time dependence of the first moment $\langle R(t)\rangle$ of the spatial distribution of the ions at time t,

$$\langle R(t)\rangle = \int rn(r,t)\mathrm{d}r \quad (1)$$

The CE dynamics is described in Fig. 7 by the time dependence of $\langle R(t)\rangle/\langle R(t_s)\rangle$, where $\langle R(t)\rangle$ is the first moment of the spatial distribution at time $t - t_s$, while $\langle R(t_s)\rangle$ is the initial value of $\langle R(t)\rangle$ at $t = t_s$. For $I_M \geq 10^{17}$ W cm^{-2}, when outer ionization is complete, a linear time dependence of $\langle R(t)\rangle$ is exhibited at longer times (Fig. 7). $\langle R(t)\rangle$ can be then approximately presented in the form

$$\langle R(t)\rangle/\langle R(t_s)\rangle = 1;\ t < t_{onset}$$
$$\langle R(t)\rangle/\langle R(t_s)\rangle = a(t - t_{onset}) + 1;\ t > t_{onset}. \quad (2)$$

The onset time t_{onset} (Table 1) is due to the completion of outer ionization, as well as to the switching-off of ion acceleration

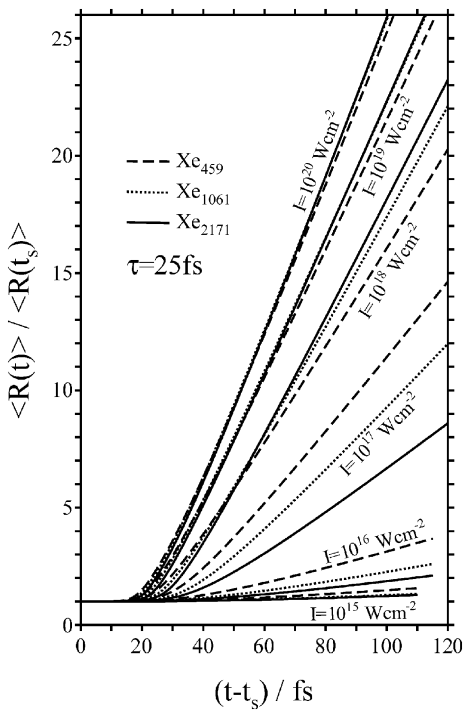

Fig. 7 Cluster size and laser intensity dependence of the spatial expansion of Xe_n clusters undergoing Coulomb explosions. The spatial expansion is characterized by the normalized first moment $\langle R(t)\rangle/\langle R(t_s)\rangle$ of the radial distribution functions, *i.e.*, normalized by the first moment $\langle R(t_s)\rangle$ at the initial time $t = t_s$. The functions $\langle R(t)\rangle/\langle R(t_s)\rangle$ are given for the Xe_{459}, Xe_{1061} and Xe_{2171} cluster in the intensity range $I_M = 10^{15}$–10^{20} W cm^{-2} and for a pulse length of τ = 25 fs.

effects.[24,33,34] Eqn (2), describes well the simulation data for all cluster sizes at $I_M = 10^{18}$–10^{20} W cm^{-2} (τ = 25 fs) and for the smaller cluster sizes of n = 459 at $I_M = 10^{17}$ W cm^{-2} (Fig. 7). The a parameter in eqn (2) represents the CE velocity. On the other hand, at lower intensities of $I_M = 10^{15}$–10^{16} W cm^{-2} (Fig. 7), the linear relation, eqn (2), is inapplicable at longer times and marked deviations from eqn (2) are exhibited.

The CE velocities (Table 1) obtained from Fig. 7 at the intensities and cluster sizes where complete outer ionization prevails,[27,36] manifest a marked cluster size dependence and a large intensity dependence, being due to unique features of CE dynamics driven by multiple ionization of many-electron elemental clusters. For complete outer ionization driven by short pulses (τ = 25 fs) we apply an electrostatic model to CE of Xe_n under CVI conditions[24,33,34]

$$a = 0.936(\rho_{Xe}/m_{Xe})^{1/2}q_{av}, \quad (3)$$

where the CE velocity a is given in fs^{-1}, ρ_{Xe} = 0.017 Å^{-3} is the initial cluster ion density (given in Å^{-3}), m_{Xe} the mass of Xe (in amu) and q_{av} is the average ionic charge (in e units). Eqn (3) predicts that $a \propto q_{av}$, so that (at fixed I_M and τ) a manifests a weak size dependence, being due to the size dependence of q_{av}. Eqn (3) is inapplicable in the lower intensity range of $I_M = 10^{15}$–10^{16} W cm^{-2} (for all values of n) and $I_M = 10^{17}$ W cm^{-2} (n = 1061, 2171), where the nanoplasma is persistent,[27,36] marking the failure of the CVI model. The results of the electrostatic model, eqn (3), with the q_{av} data (Fig. 6), account reasonably well for the simulation results (Table 1). At the highest intensities of $I_M = 10^{19}$ and 10^{20} W cm^{-2} where q_{av} is cluster size independent, eqn (3) predicts that a is independent of the cluster size in accord with the simulation results (with a decreasing only by 3%–5% in the range n = 459–2171), while the values of a at $I_M = 10^{19}$ W cm^{-2} are predicted by eqn (3) within 10%. The larger deviation of 15% between simulation results and eqn (3) at $I_M = 10^{20}$ W cm^{-2} probably originates from anisotropy in CE at this ultrahigh intensity. The 20% increase of a at $I_M = 10^{18}$ W cm^{-2} (τ = 25 fs) in the size domain n = 459–2171 (Table 1) is due to the increase of q_{av} (section II.C), being well accounted for by eqn (3). The agreement between theory and simulation for CE dynamics provides a criterion for the identification of the cluster size and intensity domain for complete outer ionization, where the expansion velocity can be described by the CVI model.

IV. Energetics of Coulomb explosion

IV.A Energetics in the CVI limit

The energetics of ions produced by CE of a $\{Xe^{q+}\}_n$ cluster under CVI conditions will be approximated by considering the uniform CE of a $(Xe^{q_{av}+})_n$ cluster. The final kinetic energy E of a $Xe^{q_{av}+}$ ion initially located at distance r from the cluster center is[10,24,33]

$$E(r) = (4\pi/3)\bar{B}\rho_{Xe}(q_{av})^2r^2; \quad 0 \leq r \leq R_0 \quad (4)$$

where $\bar{B}$ = 14.40 ev, ρ_{Xe} = 0.017 Å^{-3} is the initial density, q_{av} is given in e units (Fig. 4), r in Å and $E(r)$ in eV. From eqn (4)

Table 1 Dynamics of CE of Xe_n clusters driven by ultraintense lasers (τ = 25 fs)

I_M/W cm^{-2}	n	q_{av}	t_{onset}/fs[a]	a/fs^{-1} simulations[b]	a/fs^{-1} CVI model[c]
10^{17}	459	15.2	7.7	0.162	0.162
10^{18}	459	18.8	−3.3	0.212	0.200
10^{18}	1061	21.3	−1.2	0.238	0.227
10^{18}	2171	23.3	0.7	0.256	0.248
10^{19}	459	26.0	−9.5	0.280	0.277
10^{19}	1061	26.0	−9.1	0.292	0.277
10^{19}	2171	26.0	−8.3	0.296	0.277
10^{20}	459	36.0	−13.0	0.330	0.383
10^{20}	1061	36.0	−12.8	0.339	0.383
10^{20}	2171	36.0	−12.3	0.342	0.383

[a] Onset time, eqn (2), relative to the peak of the pulse envelope. [b] Data from Fig. 7 for intensities and cluster sizes when complete outer ionization was attained. [c] Predictions of the CVI model, eqn (3).

we infer that the average energy E_{av} and the maximal energy E_M of the ions are given by[10,24,33]

$$E_{av} = \frac{4\pi}{5}\overline{B}\rho_{Xe}q_{av}^2R_0^2 \quad (5)$$

$$E_M = \frac{4\pi}{3}\overline{B}\rho_{Xe}q_{av}^2R_0^2 \quad (6)$$

(1) Size dependence. At a fixed intensity, the cluster size dependence of the energetics, eqn (5) and (6), is $E_{av}(n)$, $E_M(n) \propto q_{av}^2R_0^2 \propto q_{av}^2n^{2/3}$, where q_{av} depends on the laser parameters and on n (section II.C). The dependence of the energies on q_{av} manifests ignition and nanoplasma screening effects in inner ionization.

(2) Intensity dependent energetic enhancement. At a fixed initial cluster size, the energies of CE are expected to increase markedly with increasing the laser intensity, with $E_{av}(n)$, $E_M(n) \propto (q_{av})^2$.

(3) Pulse length dependence. The dependence of q_{av} on τ for fixed intensity and laser size (Fig. 6) will result in the dependence of E_{av} and E_M on this laser parameter.

(4) Energy ratios. At a fixed laser parameters, the ratio

$$E_{av}(n)/E_M(n) = 5/3 \quad (7)$$

is independent of q_{av} and of n.

Of interest is the kinetic energy distribution $P(E)$ that on the basis of eqn (4) is given by[10,24,33]

$$P(E) = 3/2(E/E_M(n)^3)^{1/2};\ E \le E_M(n) \quad (8)$$

The cut-off $E_M(n)$ maximal energy and the normalization parameter $E_M(n)^{-3/2}$ in eqn (8) are given by eqn (6). These results of the electrostatic model, eqn (5)–(8), will serve as a benchmark for the analysis of the energetics where the nanoplasma is transient, and for the extension of the description for the regime where the nanoplasma is persistent.

IV.B Kinetic energy distributions

In Fig. 8 we present the simulation results for the kinetic energy distributions of the Xe^{q+} ions from CE of Xe_{2171}. The energy distribution is expressed in terms of $P(E)\delta E = n(E)\delta E/n$, where $n(E)$ is the number density of ions and δE an energy interval, which was chosen as 0.2 keV for $I_M = 10^{15}$ W cm^{-2} and as 5 keV for $I_M = 10^{18}$ W cm^{-2}. At the high intensity of $I_M = 10^{18}$ W cm^{-2} (τ = 20, 50, 100 fs), the maximal energy E_M exhibits a marked decrease with increasing τ (Fig. 8a). This effect is in accord with eqn (6), *i.e.*, $E_M \propto q_{av}^2$ together with the

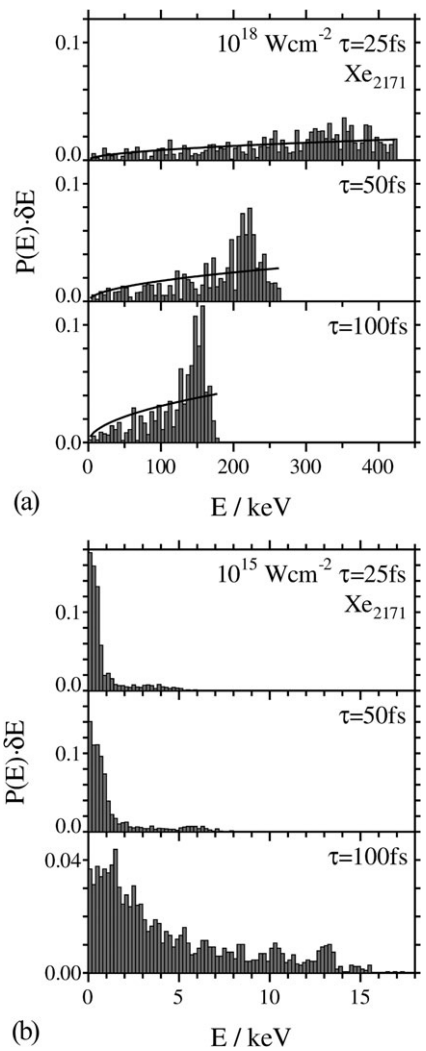

Fig. 8 The pulse length dependence of the kinetic energy distributions of Xe^{q+} ions in the CE of a Xe_{2171} cluster irradiated by a Gaussian laser pulse. (a) $I_M = 10^{18}$ W cm^{-2}. (b) $I_M = 10^{15}$ W cm^{-2}. The energy distribution functions are given for τ = 25, 50 and 100 fs laser pulses, as marked on the panels. The solid lines in Fig. 8a represent the CVI relation, eqn (8), with the maximal energies E_M obtained from the MD simulations.

pulse length dependence of q_{av} at $I_M = 10^{18}$ W cm^{-2} presented in Fig. 6, with the decrease of q_{av} with increasing τ is due to the reduction of ignition effects (sections II.B and II.C). The ratios E_M/q_{av}^2 for Xe_{2171} exhibit only a weak τ dependence, *i.e.*, $E_M/q_{av}^2 = 0.76$ keV e^{-2} at $\tau = 25$ fs, $E_M/q_{av}^2 = 0.68$ keV e^{-2} at $\tau = 50$ fs, and $E_M/q_{av}^2 = 0.58$ keV e^{-2} at $\tau = 100$ fs. At $I_M = 10^{18}$ W cm^{-2} and for a short pulse of $\tau = 25$ fs, $P(E)$ increases with increasing E (upper panel in Fig. 8a), in reasonable agreement with the CVI distribution, eqn (8). However, some positive deviations from eqn (8) are exhibited for $I_M = 10^{18}$ W cm^{-2} and $\tau = 25$ fs for $P(E)$ at higher energies below E_M (upper panel in Fig. 8a), which are tentatively attributed to the contribution to CE of the highly-charged $(Xe^{q+})_n$ ($q = 21$–25) ions initially located in the region of the cluster surface profile. This effect will be exhibited under CVI conditions, which prevail for the short $\tau = 25$ fs pulse. For longer pulses of $\tau = 50$ fs and 100 fs at $I_M = 10^{18}$ W cm^{-2} (the middle and lower panels in Fig. 8a), the simulated energy distributions exhibit a rise at lower energies (with values somewhat lower than those predicted by eqn (8)), and a marked maximum at higher energies below E_M. The maxima in $P(E)$ for $\tau = 50$ fs and 100 fs manifest marked deviations from the CVI model, eqn (8), for longer pulse lengths, when outer ionization occurs in parallel to CE. Accordingly, at $I_M = 10^{18}$ W cm^{-2} when complete outer ionization is accomplished, the time scales between electron and nuclear dynamics cannot be separated for long pulse lengths.

At the intensity of $I_M = 10^{15}$ W cm^{-2} (Fig. 8b), $P(E)$ shows a decrease with increasing E with a qualitatively different dependence of $P(E)$ on E that is expected from eqn (8) (Fig. 8b). The high energy tail of $P(E)$ can be approximately described by a thermal distribution $P(E) \propto \exp(-E/3E_{av})$. At this low intensity a persistent nanoplasma is retained within the cluster, which is characterized by a relatively low average kinetic energy of $E_{av} = 26$ eV for the electrons in a Xe_{2171} cluster.[36] This persistent nanoplasma screens the ion–ion Coulomb repulsions leading to the inapplicability of the CVI result, as will be discussed in section VI.

IV.C Average and maximal ion kinetic energies

In Fig. 9 and 10 we portray the cluster size dependence of the energetic parameters that specify P(E), *i.e.*, the average energy $E_{av} = \int EP(E)dE$ and the maximal energy E_M *vs.* R_0^2 at fixed I_M and τ. The cluster size equations $E_M \propto R_0^2$ and $E_{av} \propto R_0^2$, eqn (5) and (6), are well obeyed at $I_M = 10^{19}$–10^{20} W cm^{-2} for both $\tau = 25$ fs and 100 fs (Fig. 9a and 10), where, for a fixed I_M, q_{av} is independent of the cluster size (Fig. 6). In the intensity range $I_M = 10^{18}$ W cm^{-2} at $\tau = 25$ fs (Fig. 9a and 10), and $I_M = 10^{17}$–10^{18} W cm^{-2} at $\tau = 100$ fs (Fig. 9b), E_{av} and E_M exhibit a superlinear cluster size dependence on R_0^2, which can be traced to the increase of q_{av} with increasing the cluster size at these intensities due to ignition (Fig. 6 and section II.C). We shall now analyze the CE energetics in the intensity and cluster size domain where complete outer ionization occurs. Provided that the time scale for outer ionization is shorter than for CE, the energetics correspond to CVI conditions, eqn (5–7), which provide the scaling laws

$$E_{av}q_{av}^{-2} = \gamma_{av}R_0^2 \qquad (9a)$$

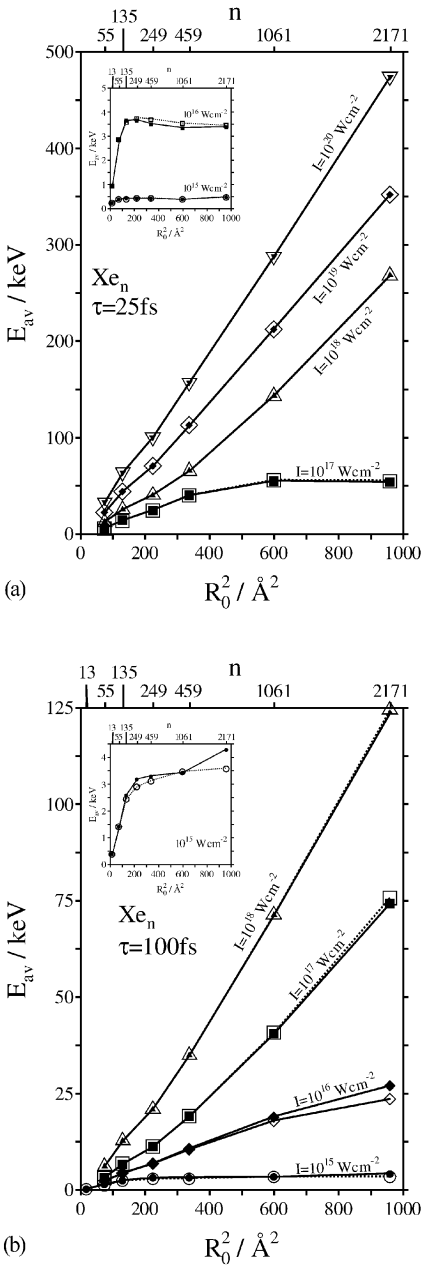

Fig. 9 The cluster size and the laser intensity dependence of the average ion energies in the CE of Xe_n clusters for different pulse lengths. The intensities are marked on the curves. The closed symbols, connected by solid lines, correspond to the full simulation results, while the open symbols, connected by dashed curves, represent simulation results with the EII channel being switched off. (a) $\tau = 25$ fs. (b) $\tau = 100$ fs.

and

$$E_M q_{av}^{-2} = \gamma_M R_0^2 \qquad (9b)$$

where the parameters γ_{av} and γ_M are independent of the cluster size, the laser intensity and the pulse width. From the simulation results for $E_{av}q_{av}^{-2}$ and $E_M q_{av}^{-2}$ presented in Fig. 11a and b, we infer that the size scaling laws, eqn (9a) and (9b), are reasonably satisfied. The R_0^2 scaling is well obeyed, however, the γ_{av} and γ_M coefficients reveal some non-systematic

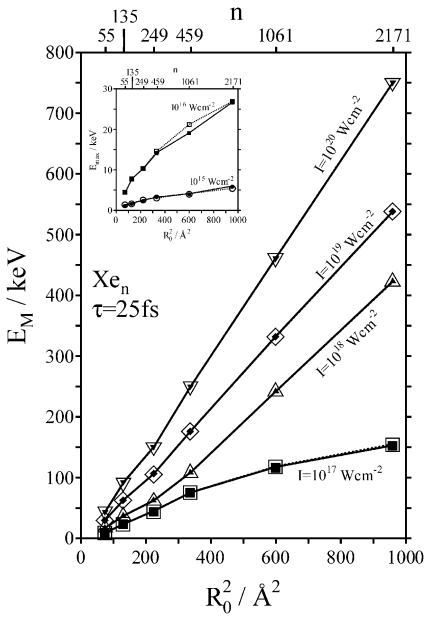

Fig. 10 The cluster size and laser intensity dependence of the maximal ion energies in CE of Xe_n clusters for $\tau = 25$ fs laser pulses. The intensities are marked on the curves. The marking of data points for full simulations and for simulations with the EII channel being switched off, are identical to those in Fig. 9.

deviations. The spread in the γ_{av} and γ_M parameters is 20% (Fig. 11a and b), while the spread of the E_{av} and E_M data at fixed cluster size corresponds to a numerical factor of 7 (Fig. 9a, b and 10). Data analysis was performed for $I_M = 10^{18}$–10^{20} W cm^{-2} at $\tau = 25$ fs and 100 fs. For the largest cluster (Xe_{2171}), for which the continuum and CVI approximations inherent in eqn (5)–(7), (9a) and (9b) are adequate, we obtained $\gamma_{av} = (4.3 \pm 0.6) \times 10^{-4}$ keV Å^2 e^{-2} and $\gamma_M = (6.6 \pm 1.0) \times 10^{-4}$ keV Å^{-2} e^{-2}. The analysis of the individual $E_M q_{av}^{-2}$ and $E_{av} q_{av}^{-2}$ simulated data for each cluster size in the range $n = 459$–2171 and I_M in the range 10^{18}–10^{20} W cm^{-2}, $\tau = 25$ fs and 100 fs, resulted in $\gamma_M/\gamma_{av} = 1.55 \pm 0.11$. These simulation results for γ_{av}, γ_M and their ratio are in reasonable, but not perfect, agreement with the predictions of the electrostatic model for CE driven by multiple ionization under CVI conditions, eqn (5), (7) and (9), which resulted in $\gamma_{av} = 6.5 \times 10^{-4}$ keV Å^{-2} e^{-2}, $\gamma_M = 10.3 \times 10^{-4}$ keV Å^{-2} e^{-2} and $\gamma_M/\gamma_{av} = 1.67$. The γ_{av} and γ_M parameters inferred from the simulations are lower by about 50% than those predicted by the CVI model, eqn (5), (6) and (9). Such deviations are not manifested for CE of $(D_2)_n$ clusters at high intensities when the CVI provides a good description of the size dependent energetics.[33] These deviations from the CVI for the energetics of Xe_n clusters, together with systematic spread of the E_{av} and E_M data in Fig. 11a and b are due to a multitude of phenomena and processes, which are disregarded in the CVI electrostatic model for an initially homogeneous cluster, *e.g.*, kinematic effects originating both from the charge distribution and the density profile at the surface, the inseparability of time scales between outer ionization and CE for longer pulses, and effects of the pulse shape on outer ionization dynamics[33]

At lower intensities, which lie below the complete outer ionization and CVI domain specified above, there is a marked

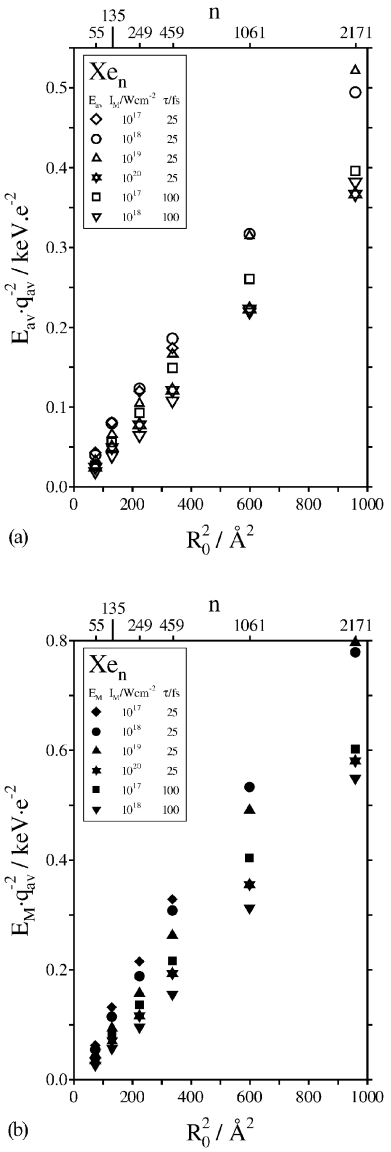

Fig. 11 Charge and cluster size scaling of the CE energies according to eqn (9a) and (9b). (a) Average energies E_{av}. (b) Maximal energies E_M. The data points for the pulse parameters are marked on the Figures.

breakdown of the linear or superlinear E_{av}, $E_M \propto R_0^2$ size dependence. At $I_M = 10^{17}$ W cm^{-2} and for $\tau = 25$ fs, a linear dependence of E_{av} and E_M on R_0^2 is exhibited only for $n = 55$–459 (Fig. 9a and 10), while for $n > 459$ a flattening of the E_{av} *vs.* R_0^2 dependence (Fig. 9a) and a linear dependence of E_M on R_0 (Fig. 10) is manifested, marking the breakdown of the CVI domain. That is to say, the maximum number $n^{(I)}$ of atoms of the CVI domain can be bracketed in the size range $n = 459$–1061 for $I_M = 10^{17}$ W cm^{-2} and for $\tau = 25$ fs. $n^{(I)}$ increases with decreasing the laser intensity, *i.e.*, for 10^{16} W cm^{-2} and $\tau = 25$ fs, $n^{(I)}$ falls in the range $n = 55$–135, and for 10^{15} W cm^{-2}, $n^{(I)} < 13$. $n^{(I)}$ at a fixed value of I_M markedly increases with increasing τ, *i.e.*, for $I_M = 10^{16}$ W cm^{-2} $n^{(I)} = 55$–135 at $\tau = 25$ fs (Fig. 9a), while $n^{(I)} = 1061$–2171 at $\tau = 100$ fs (Fig. 9b). These estimates for the cluster size for the applicability of the scaling laws for the

energetics of CE, eqn (5)–(7), will be characterized in terms of the border radius for outer ionization,[10,24,33,34,36] which will be considered in section V.

IV.D A comment on the role of electron impact ionization on the CE energetics

The complex interplay between laser BSI, inner field ignition and screening effects, and EII contributions to the ionization levels of Xe_n clusters was previously explored by us.[27,36] Information about the net effect of EII on the energetics of CE was obtained from additional simulations, in which the EII channel was switched off. From the results for E_{av} and E_M presented in Fig. 9a, b and 10 it appears that the contribution of EII to the CE energetics for $I_M \geq 10^{17}$ W cm^{-2} (τ = 25 and 100 fs) is less than 3%. This is not surprising in view of the competition between BSI and EII under these conditions[27,43] and the small contribution of EII to q_{av} and therefore also to the CE energetics in the CVI region. At lower intensities, corresponding to the non-CVI region, *i.e.*, at $I_M = 10^{16}$ W cm^{-2} with τ = 25 fs (inset to Fig. 9a), at $I_M = 10^{16}$ W cm^{-2} with τ = 100 fs (Fig. 9b), and, in particular, for n = 2171 at $I_M = 10^{15}$ W cm^{-2} with τ = 100 fs (inset to Fig. 9b), the EII by the persistent nanoplasma increases q_{av} and therefore also the CE energies. From these results we conclude that a reasonable description of the CE energetics in the cluster size domain studied herein (within an accuracy of 20%) can be obtained from simplified simulations that do not include the EII channel. The data for the lowest intensity and longest pulse studied by us (insets to Fig. 9a and b) indicate that for CE energetics of larger clusters the effects of EII may be significant in the lower intensity domain and have to be explored.

V. The border radius for outer ionization and for CVI

The border radius $R_0^{(I)}$ constitutes the maximal value of the initial cluster for which complete outer ionization is attained.[10,33,34] $R_0^{(I)}$ data for complete outer ionization of Xe_n clusters were previously obtained by two methods:[36]

(i) MD simulations of time-dependent outer ionization dynamics.[10,33,36] The outer ionization levels $n_{oi}(t)$ (per constituent atom) are related to the number of nanoplasma electrons $n_p(t)$ by $n_p(t) = n_{ii}(t) - n_{oi}(t)$, where $n_{ii}(t)$ is the inner ionization level at this time t.[26,36] Simulations of electron dynamics were used for the characterization of the initial cluster radius for complete outer ionization.[10,26,36] For short pulses (τ = 25 fs) we previously considered the maximal cluster size, which allows for complete outer ionization at the peak of the pulse, *i.e.*, $n_p(t = 0) = 0$ (which in our previous numerical procedure was taken as $n_p(t = 0) = 0.05$).[10,33,36]

(ii) An electrostatic model.[10,33,36] On the basis of the CBSI model for outer ionization, together with MD simulations of the outer ionization level, the intensity and pulse length dependence of the border radius was expressed in the form[36]

$$R_0^{(I)} = 1.09 \times 10^{-7}\, \tau^{0.64} I_M^{1/2}/q_{av} \qquad (10)$$

where I_M is expressed in W cm^{-2}, q_{av} is expressed in e units and the pulse length τ in fs units, while $R_0^{(I)}$ is given in Å. The τ^{α} dependence for Xe_n clusters ($\alpha = 0.64 \pm 0.03$) is close to the power law with $\alpha = 0.66$ obtained for outer ionization of $(D_2)_n$ clusters.[33]

For short pulses of τ = 25 fs and for higher intensities at $I_M = 10^{17}$ W cm^{-2}, the simulation results for outer ionization (method (i)) applied for $n_p(t = 0) = 0$[10,33,36] properly account for the depletion of the nanoplasma, which occurs before the peak of the pulse. For longer pulses as well as for lower intensities, a self-consistent analysis of complete outer ionization requires a modification of the previous scheme of references 10, 33, and 36. We determined the maximal cluster size for complete outer ionization at long times relative to the pulse width, *i.e.*, taking $n_p(t_L) = 0$, where t_L is the time at the end of the trajectory, which is much longer than the pulse length. In Fig. 12 we present typical results for the time dependence of $n_p(t)$ for $I_M = 10^{16}$ W cm^{-2}, τ = 25 fs and for $I_M = 10^{15}$ W cm^{-2}, τ = 100 fs. The values of the border size in terms of number of atoms $n^{(I)}$ for outer ionization were obtained from extrapolation of $n_p(t_L)$ *vs.* n to zero (insets in Fig. 12). The $n^{(I)}$ values allowed for the determination of the border radius from the relation $R_0^{(I)} = (3n^{(I)}/4\pi\rho_{Xe})^{1/3}$. In Fig. 13 we present the $R_0^{(I)}$ data obtained from outer ionization dynamics (method (i) with the $n_p(t_L) = 0$ extrapolation), which are well accounted by the CBSI model (method (ii)), eqn (10), for τ = 25 fs and for 100 fs. It is gratifying that our analysis accounts well for $R_0^{(I)}$ for both pulse lengths.

(iii) Size dependence of CE energetics. An independent method for the determination of $R_0^{(I)}$ complements the approaches based on electron dynamics (methods (i) and (ii)) and rests on the analysis of CE energetics. We established that the energetics of CE in the region of the lower laser peak intensity and the long pulse length (section IV.C) is given by the relations $E_{av} \propto R_0^{\eta}$ for the average energies with $\eta = 2$ for $R_0 \leq R_0^{(I)}$ and $\eta = 0$ for $R_0 \gg R_0^{(I)}$, while $E_M \propto R_0^{\bar{\eta}}$ with $\bar{\eta} = 2$ for $R_0 \leq R_0^{(I)}$ and $\bar{\eta} = 1$ for $R_0 > R_0^{(I)}$ These relations for $R_0 > R_0^{(I)}$ correspond to the non-CVI domain. In the lower I_M regions, the saturation of E_{av} *vs.* R_0 and the linear dependence of E_M on R_0 are observed (Fig. 9a, b and 10). Accordingly, $R_0^{(I)}$ specifies the upper size limit for the cluster size for the applicability of the CVI conditions for the CE energies. Using method (iii), the values of $R_0^{(I)}$ were independently estimated from the energetic data in Fig. 9a, b and 10, for $I_M = 10^{15}$–10^{17} W cm^{-2} at τ = 25 fs, for $I_M = 10^{15}$ W cm^{-2} at τ = 25 fs, and for $I_M = 10^{15}$ W cm^{-2} and 10^{16} W cm^{-2} at τ = 100 fs. Following the analysis of the CE energetics at lower intensities, we use the $n^{(I)}$ data presented in section IV.C to estimate the largest initial cluster radius for the prevalence of the CVI domain in terms of the relation $R_0^{(I)} = (3n^{(I)}/4\pi\rho_{Xe})^{1/3}$. Reasonable agreement was obtained between the $R_0^{(I)}$ data estimated from the size dependence of E_{av} and of E_M. As is apparent from Fig. 13, the energetics of CE of extremely charged ions from Xe_n clusters (method (iii)) leads to estimates of $R_0^{(I)}$, which are in good agreement with the $R_0^{(I)}$ values independently obtained from MD simulations of electron dynamics (method (i)) and from the CBSI model (method (ii)). The intensity and pulse length dependence of $R_0^{(I)}$ obtained from both electron dynamics and CE energetics are well accounted for by the electrostatic CBSI model. The border radius $R_0^{(I)}$ bridges between electron (outer ionization) dynamics and nuclear (CE) dynamics in elemental and molecular clusters.

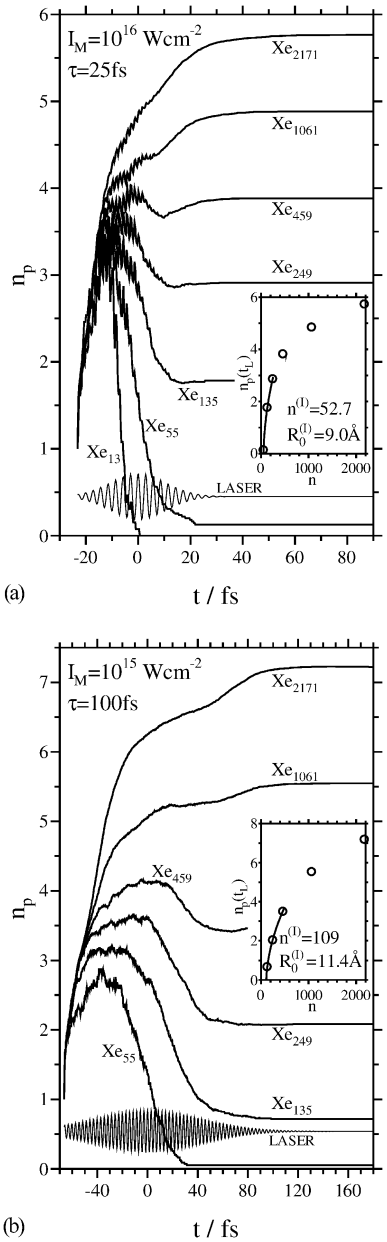

Fig. 12 Dynamics of outer ionization as specified by the time dependence of the population $n_p(t)$ of the nanoplasma for different cluster sizes at fixed I_M and τ. The insets represent the extrapolation of the size dependent $n_p(t_L)$ values to the cluster size $n^{(I)}$ at which $n_p(t_L)$ is zero. The values of $n^{(I)}$ and the corresponding cluster border radii $R_0^{(I)}$ obtained from this procedure are given in the insets. (a) $I_M = 10^{16}$ W cm^{-2}, $\tau = 25$ fs, (b) $I_M = 10^{15}$ W cm^{-2}, $\tau = 100$ fs.

VI. CE in the persistent nanoplasma domain

Under the conditions of incomplete outer ionization the laser field is not sufficiently strong to remove all the nanoplasma electrons, and CE occurs from the ionic cluster, which still contains the persistent nanoplasma (Fig. 1 and sections II.A and II.B). Simulations performed on the persistent nanoplasma[36] show that for the average kinetic energies at the pulse peak of $I_M = 10^{15}$ W cm^{-2} ($\tau = 25$ fs) are 15.2 eV for $n = 459$, 18.1 eV for $n = 1061$ and 26.1 eV for $n = 2171$.

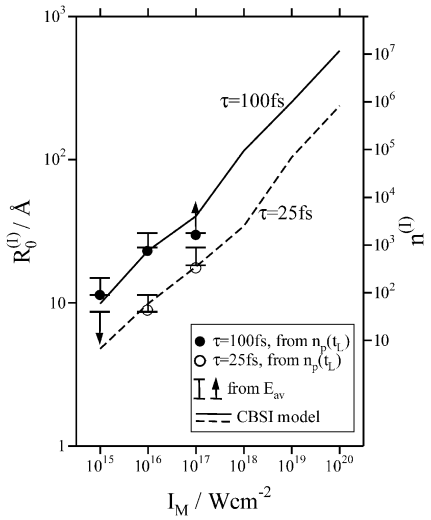

Fig. 13 The laser intensity and pulse length dependence of the border radius $R_0^{(I)}$ and of the corresponding cluster size $n^{(I)}$ for complete outer ionization of Xe_n clusters. The results of the electrostatic CBSI model (dashed line for $\tau = 25$ fs and solid line for $\tau = 100$ fs) are in good agreement with the results of the simulations of the electron dynamics (with circles and squares representing data as labeled on the Figure) and of the analysis based on the breakdown of the CVI size scaling of the average ion energies (with the bars representing uncertainty regions for the onset of the non-CVI regime, with upward (downward) arrows representing lower (upper) limits).

These electron kinetic energies are considerably lower than the electron potential energies at the cluster boundary, which falls in the range of $\sim$1 MeV for Xe_{1061}.[10,27] Accordingly, we refer to the persistent nanoplasma as a "cold" nanoplasma.[36]

We adopt the 'lychee model' previously advanced for $(D_2)_n$ clusters[35] to treat the persistent nanoplasma in Xe_n clusters, which consist of many-electron atoms. The persistent nanoplasma forms a neutral sphere with a radius R_p. The ions from the electron-free spatial exterior range $R_p \leq r \leq R_0$ undergo CE, while ions from the interior range $0 \leq r \leq R_p$ of the neutral nanoplasma are characterized by a moderately low kinetic energy. The 'lychee model' is expected to be valid for the lower intensity range of the ultraintense region, *i.e.*, $I_M \sim 10^{15}$–10^{16} W cm^{-2}, where the nanoplasma interior and exterior ionic shells are concentric. Extending previous analysis[35] the nanoplasma radius for Xe_n clusters is given in the form

$$R_p = R_0(n_p^L/q_{av})^{1/3} \quad (11)$$

where the superscript L denotes the time $t = t_L$, while the width of the ionic region $s = R_0 - R_p$ is

$$s = R_0\,[1 - (n_p^L/q_{av})^{1/3}] \quad (12)$$

Our simulations at $I_M = 10^{15}$ W cm^{-2} for the persistent nanoplasma give[36] $n_{oi}^L/q_{av} \simeq 0.22$ for Xe_{2171}, $n_{oi}^L/q_{av} = 0.17$ for Xe_{1061}, and $n_{oi}^L/q_{av} = 0.13$ for Xe_{459}. Taking $n_{oi}^L/q_{av} \ll 1$ we estimate from eqn (12) that

$$n_{oi}^L/q_{av} = 3s/R_0 \quad (13)$$

Using of the electrostatic CBSI model for the outer ionization level and for $R_0^{(I)}$ [ref. 36 and eqn (10)], we obtain

$$R_0^{(I)} = (n_{oi}^{L}/q_{av})R_0 \quad (14)$$

eqn (13) and (14) result in

$$s = R_0^{(I)}/3 \quad (15)$$

providing an approximate relation between the width of the ionic shell and the border radius.

A simple electrostatic treatment of the 'lychee model'[35] provides the following expressions for the average energy $E_{av}(R_0 \gg R_0^{(I)})$ and maximal energy $E_M(R_0 \gg R_0^{(I)})$ for CE in the intensity and cluster size domain where the persistent nanoplasma prevails

$$E_{av}(R_0 \gg R_0^{(I)}) = 6\pi\bar{B}\rho_{Xe}q_{av}^2 s^2 = (2\pi/3)\bar{B}\rho_{Xe}q_{av}^2(R_0^{(I)})^2 \quad (16)$$

and

$$E_M(R_0 \gg R_0^{(I)}) = 4\pi\bar{B}\rho q_{av}^2 s R_0 = (4\pi/3)\bar{B}\rho_{Xe}q_{av}^2 R_0^{(I)} R_0 \quad (17)$$

We note in passing that eqn (10) and (16) imply that $E_{av}(R_0 \gg R_0^{(I)}) \propto \tau^{1.28} I_M$, being independent of q_{av}. Two conclusions emerge from the application of the persistent nanoplasma model concerning the energetics of CE (for fixed I_M and τ) in the non-CVI domain. First, saturation of E_{av} is exhibited, being independent on the cluster size. Second, a linear increase of E_M on R_0 is expected. These results are in accord with the simulation results for the energetics in the non-CVI region (Fig. 9a, b and 10). eqn (16) provides a semiquantitative description of the intensity and pulse length dependence (expressed through $R_0^{(I)}$) of the saturation levels of the average energies at $R_0 \gg R_0^{(I)}$. In Fig. 14 we present the linear dependence of $E_{av}(R_0 \gg R_0^{(I)})/q_{av}^2$ *vs.* $(R_0^{(I)})^2$ in accord with eqn (16), which results in

$$E_{av}(R_0 \gg R_0^{(I)}) = \hat{\gamma} q_{av}^2 (R_0^{(I)})^2 \quad (16a)$$

with $\hat{\gamma} = 7.9 \times 10^{-4}$ keV/Å^2 e^2. This value of the proportionality parameter $\hat{\gamma}$ in eqn (16a), which was obtained from Fig. 14, is in reasonable agreement with the prediction of eqn (16) that results in $\hat{\gamma} = 5.13 \times 10^{-4}$ keV Å^{-2} e^{-2}, providing support for the applicability of the "cold" nanoplasma model for CE in the non-CVI domain.

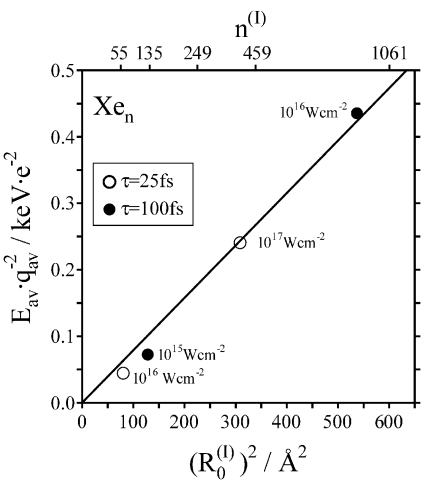

Fig. 14 The linear dependence of the asymptotic average energy $E_{av}(R_0 \gg R_0^{(I)})$ on $(R_0^{(I)})^2$ according to eqn (16a). The values of $R_0^{(I)}$ and E_{av} were obtained from MD simulations for outer ionization dynamics and for CE energetics, respectively.

The 'lychee model', which accounts for the CE energetics, asserts that the radius R_p, eqn (11), of the persistent nanoplasma is time independent on the time scale that is considerable shorter than the CE time of the exterior ionic sphere. Accordingly, the persistent nanoplasma does not spread uniformly through the expanding cluster. Our conclusions reveal the inapplicability of the 'plasma model' for outer ionization,[8,9] which implied plasmon excitation of a homogeneous charge distribution within the Coulomb exploding cluster.

VII. Concluding remarks

The unique features of CE of many-electron elemental clusters driven by multiple ionization in ultraintense and ultrafast laser fields manifest dynamics and energetics in the extreme. These extreme conditions originate from the attainment of cluster size and laser parameter dependent ultrahigh inner ionization levels, with the formation of highly charged $\{Xe^{q+}\}_n$ ionic clusters, with average charges $q_{av} = 5$–36 per ion (section II.C and ref. 27 and 43). We demonstrated that under the conditions of complete outer ionization of the nanoplasma, which were approximated in terms of the CVI initial conditions, these high ionic charges govern ultrafast dynamics and ultrahigh energetics of CE. The CE velocities scale as q_{av}, while the maximal and average energies scale as q_{av}^2. These charge scaling propensity laws, together with the CE velocities being independent of the cluster size while the CE energies obey the divergent R_0^2 ($n^{2/3}$) size scaling law, mark the CVI domain. Computational results for the CE dynamics and energetics were obtained in the cluster size range that is practical for particle MD simulations (*i.e.*, containing up to 7×10^4 ions and electrons)[25,27,37] for the currently available laser intensities (up to $I_M = 10^{20}$ W cm^{-2}).[10] The simulation results were confronted with CVI modeling. This computational-theoretical approach resulted in ultrahigh CE velocities (with the q_{av} scaling compensating for the retardation due to the $m_{Xe}^{-1/2}$ mass effect, eqn (3), which retards the ion velocities). These CE velocities fall in the range up to 15 Å fs^{-1} (Fig. 7 and Table 1), which corresponds to 0.5% of the velocity of light, providing extremely high values for nuclear motion. The highest CE energies for the largest cluster sizes and laser intensities used herein ($n = 1061$, 2171 and $I_M = 10^{20}$ W cm^{-2}) fall in the range $E_{av} = 290$ keV–480 keV and $E_M = 460$ keV–750 keV (section V). A further increase of the number of the cluster atoms by a numerical factor of 2 (*i.e.*, increasing R_0 by 1.26) will result in the formation of MeV extremely charged, *e.g.*, Xe^{36+}, ions by CE of Xe_n clusters in the moderate size domain of $R_0 = 50$ Å. MeV energies in CE of light nuclei (*e.g.*, C^{6+} or O^{8+}) require the use of nanodroplets with $R_0 = 1000$ Å–3000 Å,[28,29] reflecting on the implications of the charge and cluster size scaling for the CE energetics. Finally, we note that also other physical attributes, *e.g.*, the border radius $R_0^{(I)}$, manifest a dependence on q_{av}, *i.e.*, $R_0^{(I)} \propto q_{av}^{-1}$. In this case, the extreme inner ionization levels limit the cluster size domain for the applicability of the CVI model. High values in the range of $R_0^{(I)} = 100$ Å–400 Å can be attained only for superintense laser fields, $I_M = 10^{19}$–10^{20} W cm^{-2} (Fig. 13). The

only exception that manifests independence of a significant physical property on q_{av} pertains to the asymptotic average energy $E_{av}(R_0 \gg R_0^{(I)})$ (section VI) where a cancellation between the contributions of the charge scaling of the energetics and the border radius are exhibited.

The present study unveils new facets of the interrelationship between electron dynamics and CE nuclear dynamics and energetics. Relevant information involves the effects of laser pulse length (at fixed I_M) on the inner ionization levels (section II.B) and on the CE energetics (section IV). At $I_M = 10^{18}$ W cm^{-2}, a distribution of ionic charges with $q = 18$–25 is created by a short $\tau = 25$ fs pulse when CE is minor during the pulse, being induced by laser BSI and ignition effects. On the other hand, for a longer $\tau = 100$ fs pulse only a one-component Xe^{18+} ions are produced, manifesting the switching off of ignition effects by nuclear CE dynamics (section II.B). A marked implication of these CE dynamic processes is exhibited by the pulse length dependence of the maximal CE energies (Fig. 8a). Significant relations between electron dynamics and CE energetics are provided by the border radius $R_0^{(I)}$ (section V), which was adequately described by three independent methods: (i) MD simulations of time-dependent outer ionization dynamics; (ii) application of an electrostatic CBSI model for outer ionization; and (iii) analysis of the CE energetics in the onset of the saturation level for $E_{av}(R_0 \gg R_0^{(I)})$. It is gratifying that good agreement is obtained between the estimates of the laser intensity, laser pulse length and inner ionization level dependence of $R_0^{(I)}$, obtained from the three different approaches. In the treatment of CE energetics in the range of the existence of a persistent 'cold' nanoplasma ($R_0 \gg R_0^{(I)}$), we were able to transcend the CVI modeling. In section VI we advanced electrostatic models for the description of the properties of the persistent 'cold' nanoplasma and CE energies in the non-CVI regime for a many-electron cluster driven by laser fields in the range of $I_M = 10^{15}$–10^{16} W cm^{-2}.

A most interesting conceptual issue in the context of the interrelationship between electron and nuclear dynamics involves the correlation between complete outer ionization and the applicability of CVI initial conditions for the description of CE. From the operational point of view, the CVI model provides a satisfactory description of the CE dynamics for high intensities ($I_M = 10^{18}$–10^{20} W cm^{-2}, section III) and reasonable, though not perfect, agreement for the gross features of the energetics, *i.e.*, CE average and maximal energies driven by laser pulses with $\tau = 10$–100 fs (section IV). Of course, the applicability of the CVI model to exploding Xe_n clusters is fraught with some approximations, *e.g.*, disregarding the distribution of the ionic charges and neglecting effects of initial inhomogeneity due to the contribution of the initial surface profile (section IV.B), but these features will not be addressed at present. What we are interested in will be general signatures of the failure of CVI. A most striking deviation from CVI predictions is exhibited for the CE kinetic energy distributions at longer pulse lengths of $\tau = 50$ fs and 100 fs (Fig. 8a), which reflects on the inseparability of the time scales for electron outer ionization dynamics and nuclear CE dynamics. This separation of time scales constitutes a necessary condition for the rigorous applicability of the CVI modeling. In this context, an examination of electron outer ionization dynamics requires a closer scrutiny. The description of outer ionization processes by the electrostatic CBSI model[10,25,33,36] and the border radius [reference 36 and eqn (10)] imply that the ionization of the nanoplasma adiabatically follows the (time dependent) laser field and the increase of the cluster radius.[33] The good agreement for $R_0^{(I)}$ obtained from simulations of electron dynamics and the CBSI model implies the occurrence of outer ionization induced by the adiabatic following of the laser field and cluster size. Further theoretical work will be of interest, for the implications of this picture for pseudo-CVI behavior for the CE energetics. This approach will require the extension of the Keldysh model for atomic BSI[45] for the treatment of CBSI.

We now proceed to a brief confrontation between theory and experiment[13,39,40] for CE of Xe_n clusters. The computational-theoretical results reported herein describe the CE energetics of a cluster with a fixed size. To make contact with experimental data,[13,39,40] the cluster size distribution in the supersonic expansion[19,39] has to be taken into account. We have utilized the log-normal distribution of the cluster sizes[19,39] to calculate the size-averaged ion kinetic energy distributions, together with the averaged and maximal energies in the CE of a size distributed cluster assembly (SDCA).[42] Without alluding here to numerical procedures, a simple expression for the average energy $\overline{E_{av}}$ in a SDCA can be obtained for the non-CVI domain, where the relevant cluster radii considerably exceed $R_0^{(I)}$. On the basis of the saturation of E_{av} in this size domain, eqn (16) and (16a), we infer that in the non-CVI domain $\overline{E_{av}} = E_{av}(R_0 \ll R_0^{(I)})$, so that size averaging need not be carried out. For large Xe_n clusters ($n = 9000$ and average cluster radius $R_{av} = 45$ Å), irradiated by a pulse with $I_M = 1.5 \times 10^{16}$ W cm^{-2} and $\tau = 200$ fs, the experimental SDCA average energy is $\overline{E_{av}} = 42$ keV.[13] For these laser parameters, eqn (10) results in $R_0^{(I)} = 38$ Å, so that $R_{av} > R_0^{(I)}$ and eqn (16) and (16a) are approximately applicable. eqn (16a) was then used for an estimate of $\overline{E_{av}}(\text{theory}) = 60$ keV in the non-CVI domain, which is in reasonable agreement with the experimental result $\overline{E_{av}}(\text{expt}) = 42$ keV. This estimate of $\overline{E_{av}}(\text{theory})$ constitutes an upper limit, as the contribution from the CVI domain at $R_0 < R_0^{(I)}$ to the SDCA will result in the lowering of the estimated value of $\overline{E_{av}}(\text{theory})$. Our analysis of SDCA CE energetics and its comparison with experiment will be published elsewhere.[42] Another interesting feature of CE in ultraintense laser fields involves the anisotropy in the angular distribution (AIAD) of the Xe^{q+} ions. AIAD was previously reported in CE of completely ionized deuterium clusters, being attributed to the driving of the ions by the nanoplasma electrons.[33] AIAD in the CE of Xe_n clusters is of interest in view of the availability of experimental results.[13]

Two perspective extensions of the conceptual framework of CE in ultraintense fields will be of interest. First, from both experimental and computational points of view, it is desirable to transcend the size limit of Xe_n clusters (currently $n \approx 2000$, $R_0 \approx 30$ Å) to study ionization dynamics, nanoplasma response and CE in nanodroplets. To treat the dynamics of nanodroplets in ultraintense laser fields, a scaled electron and ion dynamics (SEID) method was advanced,[38] which is applicable to large nanostructures ($n = 10^6$–10^8 and $R_0 = 300$–3000 Å).[29] The application of the SEID method for the electron and nuclear dynamics of Xe_n nanodroplets requires the incorporation of EII, which was not considered in the original formalism.[38] Second, the dynamics and energetics of CE from a spatially

inhomogeneous transient cluster structures will be exciting. Traditional one-pulse driving of elemental Xe_n clusters studied herein considers the response of a nearly homogeneous, finite spatial structure, with some initial inhomogeneity originating from the surface profile. The optimal control of the ionization level of Xe_n clusters by pulse shaping at $I_M = 10^{14}$ W cm^{-2} was studied by Zamith *et al.*,[41] while our previous work[43] addressed control at $I_M = 10^{15}$ W cm^{-2} by increasing the pulse length, which enhances the EII ionization level. Both studies[41,43] considered control of the ionization level by the use of fixed-intensity pulses. Recently, Peano *et al.*[46,47] proposed and demonstrated a novel two-pulse irradiation scheme of homonuclear clusters using two pulses with different intensities. The first weaker pulse ($I_M = 10^{15}$–10^{16} W cm^{-2}) drives a slow CE in the presence of the persistent nanoplasma (ref. 35 and section VI) with the expanding exterior ionic region produces an inhomogeneous structure that serves as a target for the second, more intense pulse ($I_M = 10^{18}$–10^{20} W cm^{-2}), which results in extreme additional inner ionization, complete outer ionization and effective CE.[46,47] This nonuniform CE triggers kinematic overrun effects in exploding homonuclear clusters,[46–48] which were utilized to explore intracluster nuclear fusion within a single $(D_2)_n$ nanodroplet.[11] The application of this two-pulse irradiation scheme to CE of many-electron elemental clusters will unveil new features of dynamics and energetics at extremes.

Acknowledgements

This research was supported by the Deutsche Forschungsgemeinschaft (DFG) SFB 450 program on the "Analysis and Control of Ultrafast Photoinduced Processes" and by the James-Franck Binational German-Israeli program on laser–matter interactions. Joshua Jortner is grateful to the Humboldt Foundation for the gracious support of his research during visits to the Humboldt University of Berlin and to the Free University of Berlin. We are indebted to Professor Arie Zigler for providing us with a photograph of the Hebrew University 3TW Ti:sapphire ultraintense laser.

References

1 L. Lord Rayleigh, *Philos. Mag.*, 1882, **14**, 184.
2 I. Last, Y. Levy and J. Jortner, *Proc. Natl. Acad. Sci. U. S. A.*, 2002, **99**, 9107.
3 R. Neutze, R. Wouts, D. van der Spoel, E. Weckert and J. Hajdu, *Nature*, 2000, **406**, 752.
4 J. Purnell, E. M. Snyder, E. M. Wei and A. W. Castleman, Jr, *Chem. Phys. Lett.*, 1994, **229**, 333.
5 K. Sattler, J. Muhlback, O. Echt, P. Pfau and E. Recknagel, *Phys. Rev. Lett.*, 1981, **47**, 160.
6 C. Bréchignac, Ph. Cahuzac, F. Carliez and M. de Frutos, *Phys. Rev. Lett.*, 1990, **64**, 2893.
7 M. Hoener, C. Bostedt, S. Schorb, H. Thomas, L. Foucar, O. Jagutzki, H. Schmidt-Böcking, R. Dörner and T. Möller, *Phys. Rev. A*, 2008, **78**, 021201R.
8 V. P. Krainov and M. B. Smirnov, *Phys. Rep.*, 2002, **370**, 237.
9 U. Saalmann, Ch. Siedschlag and J. M. Rost, *J. Phys. B*, 2006, **39**, R39.
10 A. Heidenreich, I. Last and J. Jortner, *Analysis and Control of Ultrafast Photoinduced Processes*, ed. O. Kühn and L. Wöste, Springer-Verlag, Heidelberg, 2007, vol. 87, p. 575.
11 F. Peano, J. L. Martins, R. A. Fonesca, F. Peinetti, R. Mulas, G. Coppa, I. Last, J. Jortner and L. O. Silva, *Plasma Phys. Control. Fusion*, 2008, **50**, 124049.
12 J. Zweiback, R. A. Smith, T. E. Cowan, G. Hays, K. B. Wharton, V. P. Yanovsky and T. Ditmire, *Phys. Rev. Lett.*, 2000, **84**, 2634.
13 E. Springate, N. Hay, J. W. G. Tisch, M. B. Mason, T. Ditmire, M. H. R. Hutchinson and J. P. Marangos, *Phys. Rev. A*, 2000, **61**, 063201.
14 J. Zweiback, T. E. Cowan, R. A. Smith, J. H. Hartley, R. Howell, C. A. Steinke, G. Hays, K. B. Wharton, J. K. Krane and T. Ditmire, *Phys. Rev. Lett.*, 2000, **85**, 3640.
15 I. Last and J. Jortner, *Phys. Rev. A*, 2001, **64**, 063201.
16 G. Grillon, Ph. Balcou, J. P. Chambaret, D. Hulin, J. Martino, S. Moustaizis, L. Notebaert, M. Pittman, Th. Pussieux, A. Rousse, J. Ph. Rousseau, S. Sebbau, O. Sublemontier and M. Schmidt, *Phys. Rev. Lett.*, 2002, **89**, 065005.
17 I. Last and J. Jortner, *Phys. Rev. Lett.*, 2001, **87**, 033401.
18 I. Last and J. Jortner, *J. Phys. Chem. A*, 2002, **106**, 10877.
19 K. W. Madison, P. K. Patel, D. Price, A. Edens, M. Allen, T. E. Cowan, J. Zweiback and T. Ditmire, *Phys. Plasmas*, 2004, **11**, 270.
20 S. Karsch, S. Düsterer, H. Schwoerer, F. Ewald, D. Habs, M. Hegelich, G. Pletzler, A. Pukhov, K. Witte and R. Sauerbrey, *Phys. Rev. Lett.*, 2003, **91**, 015001.
21 S. Ter-Avetisyan, M. Schnürer, D. Schnürer, D. Hilscher, U. Jahnke, S. Busch, P. V. Nickles and W. Sandner, *Phys. Plasmas*, 2005, **12**, 012702.
22 J. Davis, G. M. Petrov and A. L. Velikovich, *Phys. Plasmas*, 2006, **13**, 064501.
23 I. Last and J. Jortner, *Phys. Rev. A*, 2005, **71**, 063204.
24 A. Heidenreich, I. Last and J. Jortner, *Proc. Natl. Acad. Sci. U. S. A.*, 2006, **103**, 10589.
25 I. Last and J. Jortner, *J. Chem. Phys.*, 2004, **120**, 1336.
26 I. Last and J. Jortner, *J. Chem. Phys.*, 2004, **120**, 1348.
27 A. Heidenreich, I. Last and J. Jortner, *J. Chem. Phys.*, 2007, **127**, 074305.
28 I. Last and J. Jortner, *Phys. Rev. Lett.*, 2006, **97**, 173401.
29 I. Last and J. Jortner, *Phys. Plasmas*, 2007, **14**, 123102.
30 S. Chelkowski, P. B. Corkum and A. D. Bandrauk, *Phys. Rev. Lett.*, 1999, **82**, 3416.
31 J. M. de Conto, *J. Phys. IV*, 1999, **9**, 115.
32 D. Atwood, *Soft X-Rays and Extreme Ultraviolet Radiation: Principles and applications*, Cambridge University Press, Cambridge, 1999.
33 I. Last and J. Jortner, *J. Chem. Phys.*, 2004, **121**, 3030.
34 I. Last and J. Jortner, *J. Chem. Phys.*, 2004, **121**, 8394.
35 I. Last and J. Jortner, *Phys. Rev. A*, 2006, **73**, 013202.
36 A. Heidenreich, I. Last and J. Jortner, *Eur. J. Phys. D*, 2008, **46**, 195.
37 A. Heidenreich, I. Last and J. Jortner, *Isr. J. Chem.*, 2007, **47**, 89.
38 I. Last and J. Jortner, *Phys. Rev. A*, 2007, **75**, 042507.
39 K. J. Mendham, N. Hay, M. B. Mason, J. W. G. Tisch and J. P. Marangos, *Phys. Rev. A*, 2001, **64**, 055201.
40 Y. Fukuda, K. Yamakawa, Y. Akahane, M. Aoyama, N. Inoue, H. Ueda and Y. Kishimoto, *Phys. Rev. A*, 2003, **67**, 061201R.
41 S. Zamith, T. Martchenko, Y. Ni, S. A. Aseyev, H. G. Muller and M. J. J. Vrakking, *Phys. Rev. A*, 2004, **70**, 011201R.
42 A. Heidenreich, I. Last and J. Jortner, to be published.
43 A. Heidenreich, I. Last and J. Jortner, *Laser Phys.*, 2007, **17**, 608.
44 I. Last and J. Jortner, *Phys. Rev. A*, 2008, **77**, 033201.
45 L. V. Keldysh, *Sov. Phys. JETP*, 1965, **20**, 1307.
46 F. Peano, R. A. Fonseca and L. O. Silva, *Phys. Rev. Lett.*, 2006, **94**, 033401.
47 F. Peano, R. A. Fonseca, J. L. Martins and L. O. Silva, *Phys. Rev. A*, 2006, **73**, 053202.
48 A. E. Kaplan, B. Y. Dubetski and P. L. Shkolnikov, *Phys. Rev. Lett.*, 2003, **91**, 143401.

